INORGANIC CHEMISTRY
FRONTIERS

RESEARCH ARTICLE

View Article Online
View Journal | View Issue

Cite this: *Inorg. Chem. Front.*, 2024, **11**, 5557

Post-synthetic modification of bis-iron(III)-μ-oxo-porphyrin prisms to enhance oxygen reduction electrocatalysis†

Daoyang Zhang, Lauren E. Rosch, Matthew R. Crawley and Timothy R. Cook *

Bis-iron(III)-μ-oxo porphyrins are known electrocatalysts for Oxygen Reduction Reaction (ORR) that favor four-electron four-proton chemistry. The facile formation of the μ-oxo motif makes forming cofacial structures straightforward unlike for other metalloporphyrins where the face-to-face geometry must be enforced by tethering groups. We have pioneered the use of coordination chemistry to obtain cofacial porphyrin ORR catalysts containing Co(II) ions. Here, we adapt our use of molecular clips for the post-synthetic modification of μ-oxo porphyrin dimers rather than as self-assembly building blocks. Although the cofacial geometry is inherent to the μ-oxo core, under ORR catalysis conditions, the dimer is rapidly cleaved, resulting in reactivity differences between traditional unclipped bis-iron(III)-μ-oxo porphyrins and our post-synthetically tethered architectures. We demonstrate our approach using two molecular clips that differ in length. The bis-iron(III)-μ-oxo precatalysts were characterized by ^{1}H NMR, ESI-MS, and molecular modeling to support the formation of cofacial prisms. Catalytic activity was studied electrochemically using cyclic voltammetry and hydrodynamic voltammetry. Whereas untethered bis-iron(III)-μ-oxo porphyrins are limited to heterogenous catalysis so that the dimeric structure is not lost upon the removal of the oxo bridge, our clipped architectures show significant catalytic current response under homogeneous conditions. Furthermore, when a shorter molecular clip is used as a post-synthetic tether, the selectivity under heterogeneous conditions is significantly enhanced: monomeric Fe(III) tetraphenylporphyrin (TPhP) generates 64.3% H_2O_2. When this same porphyrin is templated into a cofacial environment (Fe_2O TPhP) the selectivity improves to 15.8% H_2O_2. When a tetrapyridyl porphyrin analogue is post-synthetically tethered through a oxalate-bridged Rh_2 molecular clip, the selectivity improves further to 7.2% H_2O_2. In contrast, when a longer bis-hydroxybenzoquinato bridge is used in the clip, the selectivity drops back to 14.5% H_2O_2. Our most selective system also shows the highest current response and therefore our post-synthetic modification provides a kinetic enhancement as well. These results establish that straightforward coordination chemistry can be used for post-synthetic tuning of molecular ORR catalysts and when proper molecular clips are selected, marked enhancements to both selectivity and activity may be realized.

Received 14th May 2024,
Accepted 8th July 2024

DOI: 10.1039/d4qi01219d

rsc.li/frontiers-inorganic

Introduction

Many metal enzymes feature Fe-containing sites as critical functional elements, such as the heme/Cu-His active site of cytochrome *c* oxidase;[1] the Ni–Fe sulfur cluster in carbon monoxide dehydrogenase;[2] the Fe–Mo cluster cofactor in nitrogenase[3] and the heme active sites of cytochrome P450s that often act as monooxygenases.[4] A common factor between all those enzymes is that they are highly active and selective for small molecule activations and furthermore, many invoke the involvement of two or more metals during catalysis. Biomimetic inspiration from these enzymes has long been the basis for the design of small molecule catalysts as structural and/or functional models.[5,6]

Iron porphyrins have been well-studied for their ability to catalytically activate small molecules such as H_2,[7,8] O_2,[9–13] and CO_2.[14–19] Iron(III) porphyrins typically possess an axial anionic ligand or a μ-oxo bridging two metal sites, as shown in Fig. 1.[9,20–23] Fe porphyrins have been extensively studied for the Oxygen Reduction Reaction (ORR). Homogeneous ORR catalyzed by monomeric species has shown wildly different

Department of Chemistry, University at Buffalo, The State University of New York, Buffalo, New York 14260, USA. E-mail: trcook@buffalo.edu

† Electronic supplementary information (ESI) available. See DOI: https://doi.org/10.1039/d4qi01219d

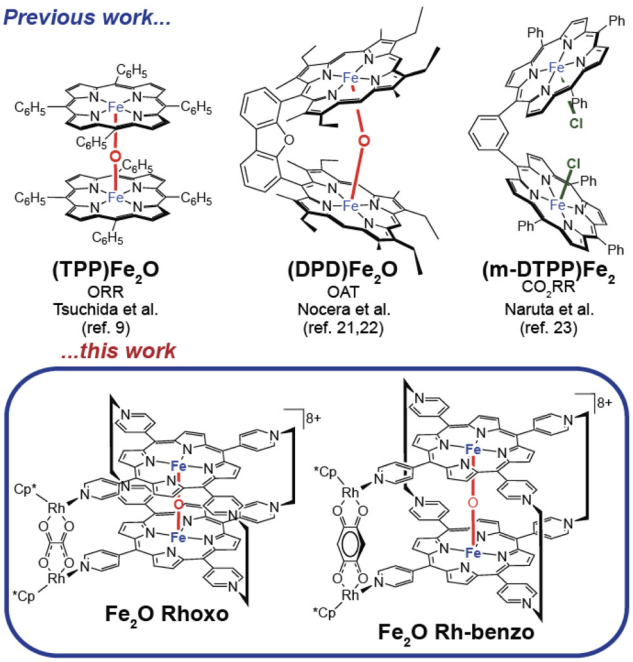

Fig. 1 Select examples of dinuclear iron porphyrins.

selectivities that vary by condition and research group. For example, Fe(II) 5,10,15,20-tetrakis(4-*N*-methylpyridyl)porphyrin has been reported to quantitatively form H_2O_2, though other studies report 100% H_2O. This inconsistent selectivity in aqueous conditions can be explained by a 2 + 2 mechanism, where a second catalytic cycle reduces the hydrogen peroxide further. Alternatively, an H_2O_2 dismutase mechanism may be active. In DMF, Mayer and coworkers have provided a detailed mechanistic analysis of ORR by Fe tetraphenyl porphyrin in which the first proton transfer is rate-limiting and selectivity for H_2O is high as a result.[24] In contrast, when a cofacial environment is present, molecular oxygen can undergo authentic four-electron four-proton chemistry and as such, existing bis-iron(III)-μ-oxo porphyrins are most commonly studied as heterogeneous catalysts in aqueous conditions. In solution, these dimers dissociate to monomeric species during turnover but in the solid-state, hindered molecular motion maintains the necessary cofacial clefts.

One strategy to maintain a cofacial cleft independent of a μ-oxo bridge or heterogeneous conditions is to formally tether the two porphyrins. This approach has been most extensively used to increase the selectivity and activity of Co-based ORR catalysts, for example Co FTF_4, which contains four amide-based covalent linkers.[25–27] We have used coordination-driven self-assembly for the synthesis and systematic tuning of multi-porphyrin architectures based on pioneering designs by Guo-Xin Jin,[28,29] Bruno Therrien,[30,31] and Jonathan Nitschke,[32,33] adapting them for ORR catalysis using Co(II) while controlling the length of the tethers,[34–36] nuclearity,[37] symmetry and stoichiometry,[38] and rigidity.[39]

Studies of analogous diiron architectures are underdeveloped. Nocera and coworkers investigated O-atom transfer chemistry using so-called Pacman porphyrins where a reactive Fe(IV)-oxo could be exposed upon photolysis of the μ-oxo bridge,[21,22,40–43] building upon Balch's work on untethered μ-oxo dimers that established this reactivity.[42,43] Naruta and coworkers explored CO_2 reduction electrocatalysis using a similar Pacman structure.[23] To the best of our knowledge, there are no reports of tethered cofacial iron porphyrins as ORR catalysts despite the high selectivity of untethered Fe(III) μ-oxo dimers under heterogeneous conditions. In 2017, Tanaka and coworkers reported a cofacial porphyrin/phthalocyanine architecture that was ~98% selective for H_2O as an electrocatalyst for ORR.[44]

Herein, we adapt our coordination-driven self-assembly approach as a method to post-synthetically modify bis-iron(III)-μ-oxo-porphyrin prisms. There is a growing interest in externally controlling catalysis *via* post-synthetic coordination that does not alter the primary environment of active metal sites. For example, binding cations to crown ethers can promote phase transfer,[45,46] can gate substrate access,[47] and can impart conformation control.[48] We now show how dinuclear molecular clips can be used for conformational control of tetrapyridylporphyrins to enforce cofacial geometries independent of μ-oxo bridges. We have fully characterized these novel architectures and established their ORR reactivity against monomeric and unclipped μ-oxo analogues under homogenous (acetonitrile) and heterogeneous (aqueous) conditions. The selectivities and kinetics of ORR were sensitive to the lengths of the molecular clips. Notably, when an oxalate-bridged molecular clip was used, four-electron four-proton chemistry was favored (92.8% H_2O). This work establishes that diiron porphyrin ORR catalysts may be tuned and enhanced using straightforward post-synthetic modifications *via* coordination chemistry, enforcing well-defined cofacial cavities both in solution and in the solid state that are highly active and selective.

Experimental

Materials

Chemicals were purchased from commercial sources and used as received unless otherwise noted. The porphyrins were prepared following a literature procedure.[21,24,49,50] Solvents were purified using a solvent-drying system (Pure Process Technology). ^{1}H NMR spectra were acquired on a Varian Inova 500 MHz spectrometer. Chemical shifts (δ) are reported in parts per million (ppm) and referenced against the residual proton resonances of the deuterated solvent. Mass spectra were recorded on an electrospray ionization (ESI) linear ion trap (LTQ)-Orbitrap XL mass spectrometer (Thermo Fisher Scientific) or by electrospray ionization using a home-built sprayer into a Bruker SolariX 12 T FT ion cyclotron resonance mass spectrometer (12 T FT-ICR) equipped with a dual source. No precautions were taken to exclude air (O_2 or water) from self-assembly reactions. UV-vis spectroelectrochemistry experiments were measured using a Pine Research WaveDriver 40 and an Avantes AvaSpec UV-vis spectrophotometer. A Pine hon-

eycomb UV-vis spectrochemical cell consisting of a built-in platinum honeycomb working electrode and a platinum counter electrode was used. Homogeneous CV experiments were carried out in dry acetonitrile solution with 100 mM $TBAPF_6$ as the supporting electrolyte. During the electrochemistry measurements, $Ag/AgNO_3$ was used as a pseudo-reference electrode. At the end of measurements, a spatula tip of ferrocene was added to the solution to convert the potentials to the ferrocene/ferrocenium couple (FcH/FcH^+). Heterogeneous electrochemistry experiments were carried out in DI water on catalyst inks with 0.5 M H_2SO_4 as the electrolyte and proton source. Ag/AgCl was used as a reference electrode. Catalyst ink film preparation: in a 2-dram vial, 1.0 μmol of dimer (Fe_2O Rhoxo, Fe_2O Rh-benzo, $(FeTPhP)_2O$) or 2.0 μmol of monomer (FeTPhPCl), 5.0 mg of carbon black, 100 μL of ethanol, and 500 μL methanol were sonicated for 1 hour. The solvent was then evaporated *in vacuo*, followed by the addition of a 70 μL Nafion solution (5% w/w in isopropanol) and 600 μL of ethanol. The resulting suspension was sonicated for 1 hour. The Nafion catalyst ink was then pipetted onto the working electrode. When CV were acquired using a 3 mm working electrode, 2 μL was drop-cast onto the surface and allowed to stand in air until dry. In the case of the larger glassy carbon disk for the ring-disk electrode, 3 μL were used to completely cover the surface. UV-vis spectroelectrochemistry experiments were carried out in dry DMF solution with 100 mM $TBABF_4$ as electrolyte. $Ag/AgNO_3$ was used as a reference electrode.[51,52]

Synthetic procedures

Iron(III) tetraphenylporphyrin chloride. The molecule was prepared by following literature procedure with slight modification.[21,24] A solution of tetraphenylporphyrin (200 mg, 0.33 mmol) in DMF (50 mL) was stirred in a round bottom flask and brought to reflux. $FeCl_2{\cdot}4H_2O$ (320 mg, 1.6 mmol, 5 equivalents) was then added to the reaction flask as a solid. The reflux was continued overnight. The crude mixture was then cooled, and the solvent was removed under reduced pressure, resulting in a dark solid. The dark solid was suspended in chloroform (~50 mL), washed with brine (3 × 50 mL), and dried over Na_2SO_4. The solution was filtered and concentrated under reduced pressure to ~10 mL. Excess hexane (~20 mL) was added to precipitate a solid that was collected by centrifugation and washed with hexane to yield the product as a dark brown solid (yield: 177 mg, 76.3%). In ^1H NMR spectra, the appearance of the paramagnetically shifted pyrrolic CH peak at ~82 ppm and disappearance of the pyrrolic NH peak at ~−2.9 ppm indicate the successful metalation of the free base porphyrin.

Iron(III) tetrapyridylporphyrin chloride. The compound was obtained using the same procedure as iron(III) tetraphenylporphyrin chloride. The product was obtained as a dark brown solid (yield: 126 mg, 53.9%).

Bis-iron(III) tetraphenylporphyrin μ-oxo. A literature procedure was adapted for the synthesis of this molecule.[21,24] A solution of iron(III) tetraphenylporphyrin chloride (50 mg, 0.71 mmol) in DCM (10 mL) was added to an aqueous NaOH solution (10 mL, 1.0 M) in a 20 mL vial. The solution was stirred overnight at room temperature. Afterwards, the organic layer was diluted to 50 mL with DCM, washed with water (3 × 50 mL), and then dried over Na_2SO_4. The solution was filtered and concentrated under reduced pressure to ~5 mL. Excess hexane (~15 mL) was added to precipitate a solid. The solid was collected by centrifugation and washed with hexane to yield the product (43.8 mg, 91.3%) as a dark green solid. In ^1H NMR spectra, the appearance of the pyrrolic peak at ~13.5 ppm and disappearance of the paramagnetically shifted pyrrolic peak at 82.5 ppm indicate the successful formation of the antiferromagnetically coupled Fe_2O species.

Bis-iron(III) tetrapyridylporphyrin μ-oxo ($(FeTPyP)_2O$). The compound was obtained by using the same procedure as iron(III) tetraphenylporphyrin chloride. The product formed as a dark green solid (42.9 mg, 89.7%).

Fe_2O Rhoxo. Rhoxo clip (20 mg, 0.0319 mmol. 4 equiv.) was combined with AgOTf (17.7 mg, 0.69 mmol. 8.8 equivalents) in 10 mL of methanol with the exclusion of light. This solution was stirred for 3 h, prompting the formation of AgCl which was removed *via* filtration through a pipet plugged with glass fiber. The filtrate was added directly to a suspension of the Fe_2O TPyP (10.7 mg, 0.0079 mmol, 1 equivalent) in 5 mL of methanol. This final mixture was refluxed for 48 h after which it was cooled and filtered once more through a pipet plugged with glass fiber to remove any insoluble byproducts. The remaining solvent was removed by rotary evaporation. The crude product was recrystallized by dissolution in methanol followed by the addition of diethyl ether. The solid was collected by centrifugation to yield the product (30.2 mg, 78.9%) as a dark green solid.

Fe_2O Rh-benzo. Rh-benzo clip (5 mg, 0.0073 mmol. 4 equiv.) was combined with AgOTf (4.1 mg, 0.016 mmol. 8.8 equivalents) in 5 mL of methanol with the exclusion of light. This solution was stirred for 3 h, prompting the formation of AgCl which was removed *via* filtration through a pipet plugged with glass fiber. The filtrate was added directly to a suspension of Fe_2O TPyP (2.50 mg, 0.0018 mmol, 1 equivalent) in 2 mL of methanol. This final mixture was refluxed for 48 h upon which it was cooled and filtered once more through a pipet plugged with glass fiber to remove any insoluble byproducts. The remaining solvent was removed by rotary evaporation. The crude product was recrystallized by dissolution in methanol followed by the addition of diethyl ether. The solid was collected by centrifuge to yield the product (7.6 mg, 82.7%) as a brownish green solid.

Results and discussion

Synthesis and characterization

The iron(III) tetrapyridyl porphyrin (**FeTPyPCl**) was synthesized by refluxing $FeCl_2$ with tetrapyridyl porphyrin in DMF; the dimerization occurred within a biphasic mixture of FeTPyPCl in DCM and 1 M NaOH in H_2O that was stirred at room temperature to form **$(FeTPyP)_2O$**. A post-assembly modification of

the dimer core with rhodium-based molecular clips prepared by following a literature procedure[53] (**Rhoxo clip** or **Rh-benzo clip**) produced clipped Fe_2O prisms (Scheme 1). No precautions were taken to exclude air (O_2 or water) from the post-assembly reactions.

NMR analysis

Monomeric Fe(III) porphyrins are paramagnetic and their ^{1}H NMR spectra often have broad features and significant downfield shifts relative to diamagnetic species. Metallated tetrapyridyl porphyrins have three types of proton resonances arising from the pyrrolic protons, and the α- and β-pyridyl protons. The pyrrolic signal for **FeTPyPCl** is found at 83 ppm, as shown in Fig. S3 and S4.† Once a dimer is formed with a μ-oxo bridge, the chemical shifts are more straightforward as the paramagnetic effects are lessened due to coupling between the two Fe(III) centers. For **Fe_2O Rhoxo**, the pyrrolic peaks shift back to ~14 ppm and appear as a broad singlet (Fig. 2). The resonances corresponding to protons on the Cp* occur at ~2 ppm. The resonances of the pyridyl protons occur between 7.5 and 9.5 ppm. The resonances associated with pyrrolic protons occur around ~14.5 ppm and are broadened due to proximity to the iron(III) center. The more distant α-protons of the pyridyl moiety occur between 8.5 and 9.5 ppm and are significantly sharper than that of the β-protons at 7.5–8.5 ppm (Fig. 2). The integrations of these peaks match the expectation of 120 protons for the Cp* groups, 32 total pyridyl protons, and 16 pyrrolic protons (Fig. 2) for our proposed structures containing two porphyrins and four molecular clips.

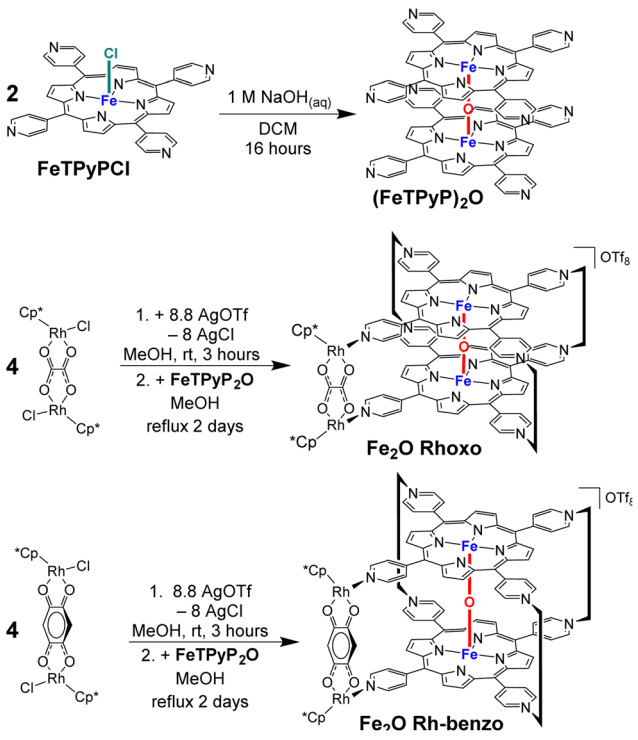

Scheme 1

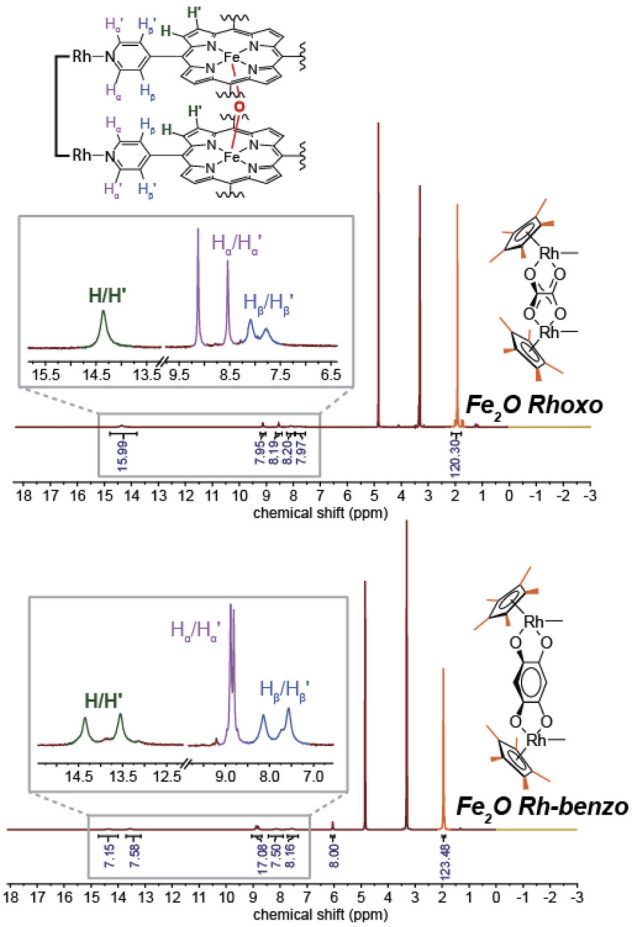

Fig. 2 ^{1}H NMR (CD_3OD, 500 MHz) of Fe_2O Rhoxo Prism (top) and Fe_2O Rh-benzo Prism (bottom). Pyridyl protons are shown in purple and blue in the insets. Pyrrolic protons are shown in green in the insets. Cp* protons are shown in orange in the full spectra.

Although many of the features of **Fe_2O Rh-benzo** are like its shorter-clipped counterpart, there are a few important distinctions. In this prism, the three types of protons on the porphyrin all split into six resolvable peaks. There are two pyrrolic proton environments, two α-proton environments, and two β-proton environments, in contrast to monomeric metalated tetrapyridyl porphyrin where these features would collapse to three total signals. This splitting to six peaks is consistent with our previous studies of a diamagnetic Zn Rhoxo prism,[38] and is rationalized by a twisting of the porphyrin faces that breaks the D_{4h} symmetry. This twisting occurs across all our family of clipped cofacial porphyrin prisms,[35,36,38] however in the case of these Fe prisms, the porphyrin–porphyrin separation is strongly enforced because of the μ-oxo bridge.

Crystal structures of unclipped Fe_2O dimers show metal–metal separations of ~3.5 Å.[54] Since this distance is shorter than the metal–metal separation in the molecular clips, the porphyrins must twist so that the pyridyl groups properly match the Rh–Rh separation. For **Fe_2O Rhoxo** the twist is small and the pyrrolic proton environment is similar, resulting in a single broad feature that corresponds to both protons;

however, for **Fe_2O Rh-benzo** this twist is significant and results in one of the pyrrolic protons being oriented towards the clipped cleft where it can be shielded by the π-cloud of the bridging 2,5-dihydroxy-1,4-benzoquinato group, while the other is directed to a clip-free cleft (see H and H′ Fig. 3). Because the environments are so different, the two unique peaks are easily resolved, with one shifting upfield due to the shielding.

The structures of both clipped prisms were optimized using ORCA 5.0.3 at the r^{2}SCAN-3c level of theory with the def2-mTZVPP basis set and are consistent with the conclusions drawn from the NMR data that the twisting of the porphyrin faces in **Fe_2O Rh-benzo** is greater than that of **Fe_2O Rhoxo** (Fig. 4).[55,56]

Mass spectrometry

High-resolution mass spectrometry (HR-MS) was used to verify the stoichiometry and elemental composition of the self-assembled cofacial structures. As shown in Fig. 5, the top red of the **Fe_2O Rhoxo** contains a 3+ peak at 1453.7 and a 4+ peak at 1053.1, arising from fully intact cores (iron porphyrin dimer clipped by four **Rhoxo clips**) that were ionized by the loss of three or four outer sphere triflate counterions, respectively. A few other peaks can be assigned that result from further fragmentation. For instance, a 3+ peak at 1166.419 is consistent with the loss of a single Rhoxo clip as well as three triflates. The bottom green trace in Fig. 5 is the HR-MS of **Fe_2O Rh-benzo**, with a 3+ peak at 1521.1 and a 4+ peak at 1103.6 due to fully intact cores (two porphyrins, four molecular clips) that have lost three and four triflate counterions, respectively. The dominant peaks for both prisms consistent with two porphyrins and four molecular clips, along with the high symmetry NMR that show distinct pyrrolic environments strongly support our structural assignment of bis-iron(III)-μ-oxo porphyrins where the molecular clips span both macrocycles. It is possible for clipped porphyrins to form bow-tie structures where the bridge spans two pyridyl groups of the same macrocycle.[57] In our prisms, the molecular clips are too rigid and short to accommodate the severe distortions that would be required for bowtie structures (see Fig. S29† for a simple molecular model showing). Examples where these clips can bridge two pyridyl sites on the same molecule have N–N separations of ~6.7 Å.[58] In TPyP, the separation is 10.9 Å.

Paramagnetic DOSY NMR were acquired (Fig. S5 and S6†) to further support the formation of singular species. Although some broadened peaks could not be resolved, all signals for **Fe_2O Rhoxo** and **Fe_2O Rh-benzo** appear with the same diffusion coefficients that also line up well with the signal

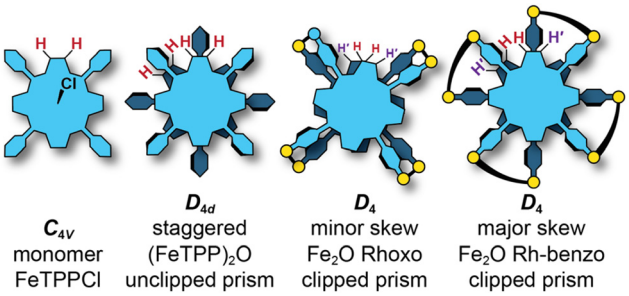

Fig. 3 Examples of different symmetries for porphyrin architectures depending on the extent of twisting. (a) Monomeric **FeTPhPCl**. (b) Unclipped Fe_2O porphyrin dimer. (c) **Fe_2O Rhoxo**. (d) **Fe_2O Rh-benzo**.

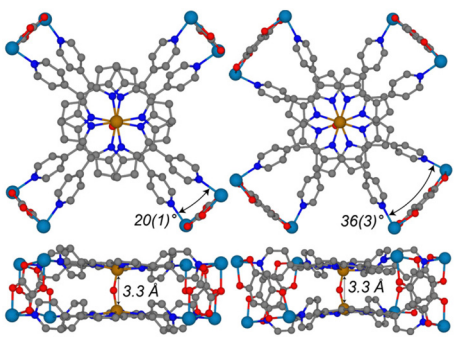

Fig. 4 Optimized structures of Fe_2O Rh-benzo and Fe_2O Rhoxo.

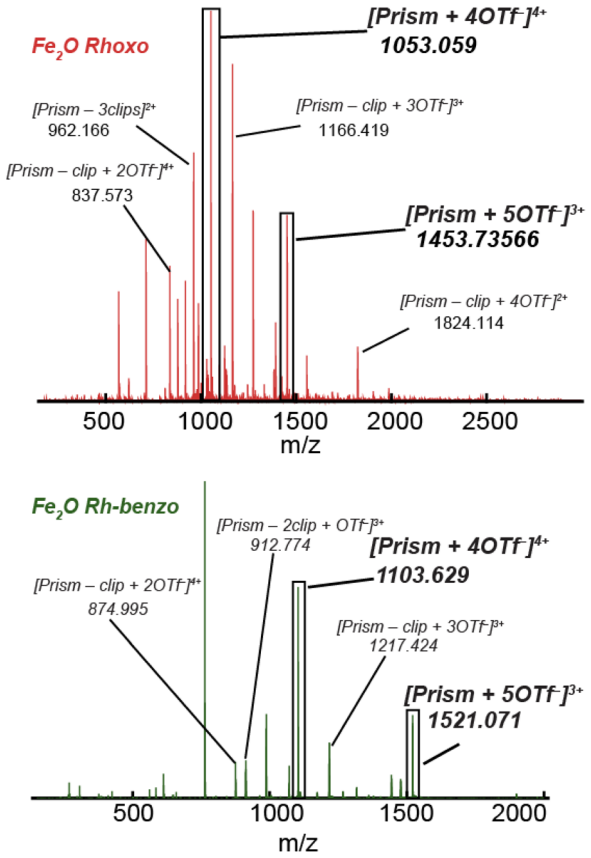

Fig. 5 High resolution mass spectra of **Fe_2O Rhoxo** (top) and **Fe_2O Rh-benzo** (bottom). "Prism" accounts for the mass of two porphyrins and four molecular clips. The number of counterions remaining are listed for each peak. Bolded labels correspond to peaks for intact prisms while non-bolded labels refer to fragments peaks that have lost molecular clips in addition to counterions.

from the Cp*, supporting that the porphyrin and clip are found in a single molecular species. The diffusion coefficients associated with these prisms is similar to what was observed for our diamagnetic **Zn Rhoxo prism**,[38] as expected for structurally related cofacial porphyrins.

Electrochemical analysis

ORR catalyzed by metallated porphyrins or related complexes often proceed by one of two pathways: a four-proton/four-electron route to generate H_2O, or a two-proton/two-electron path to form H_2O_2. To investigate the catalytic activities of these iron complexes, we conducted homogenous cyclic voltammetry experiments under four different conditions as summarized by different color traces in Fig. 6: blue (N_2, catalyst), red (O_2, catalyst), purple (N_2, trifluoroacetic acid (TFA), catalyst), and green (O_2, TFA, catalyst). Under N_2 atmosphere, there was no catalytic response. Under O_2, a reversible superoxide formation at the glassy carbon working electrode was observed with an $E_{1/2}$ value of −1.2 V *versus* FcH^+/FcH. With N_2 and TFA present as proton source, a catalytic wave was seen with an onset of −1 V *vs.* FcH^+/FcH that we ascribe to the hydrogen evolution reaction (HER). Finally, under O_2 atmosphere with TFA present, an appreciable current response was observed with an onset far more positive than that for HER, which we attributed to the oxygen reduction reaction, consistent with other cofacial porphyrins we have studied.[35,36]

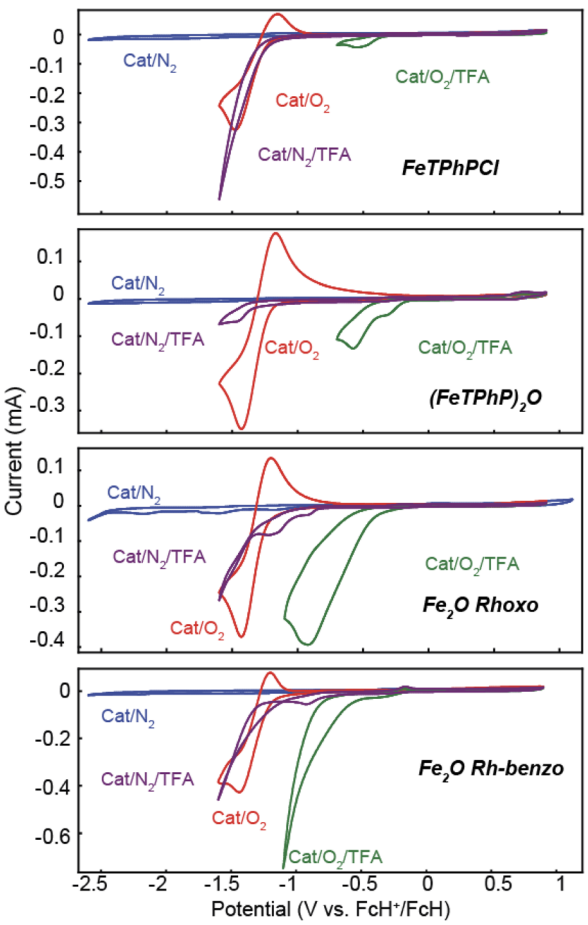

Fig. 6 CVs of Fe catalysts under homogeneous conditions. Blue: 0.2 mM monomeric porphyrin, or 0.1 mM of iron dimer (0.2 mM iron sites) under N_2 atmosphere. Red: 0.2 mM iron sites, O_2 atmosphere. Purple: 0.2 mM iron sites, N_2 atmosphere, 100 mM TFA. Green: 0.2 mM iron sites, O_2 atmosphere, 100 mM TFA. In all cases, dry acetonitrile with 100 mM $TBAPF_6$ was used. Scan rate: 100 mV s^{-1}, scan direction: reduction first. $Ag/AgNO_3$ pseudo reference electrode, data later referenced to FcH^+/FcH upon addition of ferrocene.

By comparing the current responses of monomer, unclipped dimer, and clipped dimers, we can gain some insight about the influence that post-assembly modification can have on the ORR chemistry of bis-iron(III)-μ-oxo porphyrins. The **$(FeTPhP)_2O$**, **Fe_2O Rhoxo** and **Fe_2O Rh-benzo** all have onset potentials that are more positive than that of monomeric **FeTPhPCl**; the onset potentials of all three bis-iron(III)-μ-oxo porphyrins (unclipped and two clipped dimers) are similar, suggesting that the monomer proceeds through a different mechanism than the dimers. Compared to our previously reported Co-based cofacial porphyrins, these prisms have a ~200 mV higher overpotential for ORR under identical conditions, as shown in Fig. S19.† Other metrics for ORR catalysis by the Fe systems studied here and the analogous **Co_2 Rhoxo** are summarized in Table 1.

To further interrogate ORR reactivity, faradaic efficiencies, numbers of electrons transferred, and kinetic rate constants were determined under heterogeneous conditions wherein the catalysts were immobilized along with carbon black and Nafion. The catalyst inks were cast on the surface of glassy carbon electrodes (GC), either for three-electrode measurements or hydrodynamic voltammetry using a ring disk electrode (RDE, GC disk, platinum ring). A detailed procedure is described in the ESI.† Cyclic voltammograms in 0.5 M H_2SO_4 were collected under both N_2 and O_2 atmospheres. Under the potential window of interest, no background HER was observed and all current response was attributed to ORR (Fig. S11–S14†).

Linear sweep voltammetry (LSV) was carried out with catalyst inks immobilized on the disk of an RRDE (Fig. 7). For **FeTPhPCl**, **$(FeTPhP)_2O$**, and **Fe_2O Rh-benzo**, over the potential window of interest, catalysis was kinetically limited, and no plateaus were observed to signal mass-transfer limitations. In contrast, over the same potential window **Fe_2O Rhoxo** began to exhibit a plateau in current, consistent with a depletion of O_2 at the electrode, serving as a qualitative indicator that this

Table 1 Parameters of iron(III) catalysts inks determined by electrochemical analyses

Catalyst	E_{onset}	N_{app} [b]	$\%H_2O_2$ [a]	$\%H_2O$
FeTPhPCl	0.25 V	2.7	64.3%	35.7
$(FeTPhP)_2O$	0.31 V	3.7	15.8%	84.2%
Fe_2O Rhoxo	0.32 V	3.9	7.2%	92.8%
Fe_2O Rh-benzo	0.32 V	3.7	14.5%	85.5%
Co_2 Rhoxo	0.40 V	3.7	14.5%	85.5%

[a] Determined based on the following equation: $\%H_2O_2 = \frac{2\frac{i_{ring}}{N}}{i_d + \frac{i_{ring}}{N}} \times 100$. [b] Determined based on the following equation: $N_{app} = 4 - 2\frac{(\%H_2O_2)}{100}$.

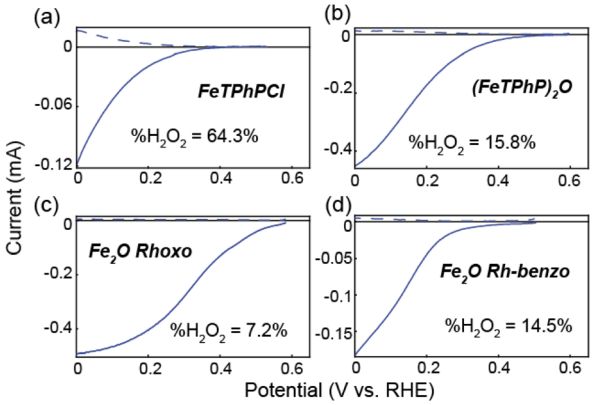

Fig. 7 RRDE voltammograms at scan rates of 20 mV s^{-1}. In all cases, the catalysts were immobilized in Nafion inks with carbon black and immersed in 0.5 M H_2SO_4. The ring potential was held at 1 V. Scan direction: reducing. (a) **FeTPhPCl**, (b) **$(FeTPhP)_2O$**, (c) **Fe_2O Rhoxo**, (d) **Fe_2O Rh-benzo**.

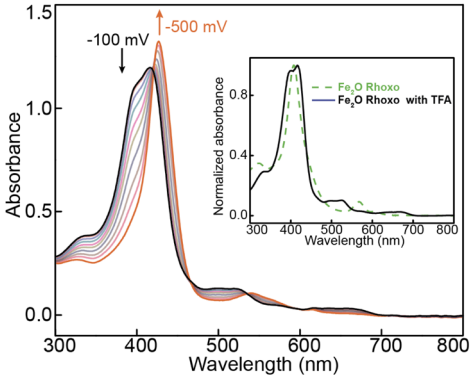

Fig. 8 Spectroelectrochemical measurements of 0.016 mM of **Fe_2O Rhoxo**, 100 mM $TBABF_4$, 100 mM TFA, DMF. Initial potential: −100 mV *vs.* Ag/Ag^+, final potential: −0.500 V *vs.* $Ag/AgNO_3$. Step amplitude: 0.050 V, step period: 30 seconds. Inset: Absorbance spectra of **Fe_2O Rhoxo** in DMF (green dashed) and with 100 mM TFA (black solid).

catalyst promotes faster ORR than the other species. By comparing disk and ring current responses, where H_2O_2 generated at the disk was oxidized at the ring, we extracted selectivity information. The monomeric **FeTPhPCl** was the least selective system for H_2O, favoring H_2O_2. All three bis-iron(III)-μ-oxo structures were significantly more selective. However, the impact of post-assembly modification with a properly selected clip is significant. For the unclipped **$(FeTPhP)_2O$**, the selectivity improved to 15.8% H_2O_2. Clipping with the larger benzo-spaced bridge showed only a modest improvement to 14.5%, which matched the selectivity of our previously studied **Co_2 Rhoxo**. When the shorter clip was used for post-assembly modification, the selectivity was greatly enhanced, with only 7.2% H_2O_2 generated.

A Koutecký–Levich (KL) analysis was carried out for the **Fe_2O Rhoxo** (Fig. S20–S25†). Since a plateau region is needed for this analysis, kinetic parameters were not extracted for **FeTPhPCl**, **$(FeTPhP)_2O$**, and **Fe_2O Rh-benzo** as scanning more negative would introduce current response from HER. The standard rate constant measured for **Fe_2O Rhoxo** was 2.3×10^2 M^{-1} s^{-1}, which is on the same order as that measured for **Co_2 Rhoxo** (2.6×10^2 M^{-1} s^{-1}).[38]

UV-vis spectroelectrochemistry

To probe the mechanism of catalysis by **Fe_2O Rhoxo**, spectroelectrochemical experiments were performed. Fig. 8 shows the UV-vis spectra recorded at different applied potentials to a honeycomb electrode placed in a solution of the cofacial porphyrin in DMF with 100 mM $TBABF_4$. The inset of Fig. 8 shows the spectral response when the **Fe_2O Rhoxo** is placed in the acidic DMF solution without any applied potential. The well-defined Soret band splits into two peaks, which is consistent with the reactivity of Fe_2O cores with acid wherein the oxo is protonated to yield an Fe(III)–OH and a solvated second Fe(III) center; thus, two distinct porphyrin absorptions are observed.[9] Upon reduction, the two Soret bands at 416 nm and 398 nm collapse back to a single peak at 426 nm while maintaining an isosbestic point, indicative of a clean transformation of the Fe(III)–OH and Fe(III)-solvated porphyrins to identical Fe(II) centers.

Proposed mechanism

Prior descriptions of the mechanism of Fe_2O dimers as ORR catalysts conclude that the oxo-bridge templates a cofacial cleft that is maintained under heterogeneous conditions where the porphyrin sites are largely immobile. In other words, even though the oxo bridge is lost upon acidification and there is no intramolecular bridge between the two porphyrin sites, the porphyrin–porphyrin separation is already fixed. Fe_2O dimers are overwhelmingly studied in the solid state because the loss of the oxo bridge under homogenous conditions means that under the conditions of catalysis (*i.e.* acid present) only monomers will persist.

When the cofacial arrangement is maintained either by immobilization or, in our case, by post-assembly clipping the two porphyrins, a subsequent reduction will provide a bis-iron(II) cavity poised for ORR. This $Fe(II)_2$ state represents an entry into the catalytic cycle shown in Scheme 2, which favors four proton/four electron chemistry. The $Fe(II)_2$ binds O_2 to give a μ-peroxo $Fe(III)_2$ species and both iron centers can be converted to Fe(III)–OH upon the addition of two more protons and electrons. A second two-proton two-electron step releases water and restores the $Fe(II)_2$ active species. In contrast, mononuclear iron porphyrins favor two proton/two electron chemistry because O_2 binds to furnish an Fe(III)-superoxo with no second metal to assist in breaking the O–O bond.

This mechanism is operative in the solid state for **$(FeTPhP)_2O$**, **Fe_2O Rhoxo**, and **Fe_2O Rh-benzo**, yet all three systems do not display the same kinetics and selectivity. From our NMR data and computational results, the **Fe_2O Rh-benzo** exhibits a more significant twist that will impact orbital overlap associated with interactions with substrate and metal–metal electronic communication. Furthermore, once the μ-oxo

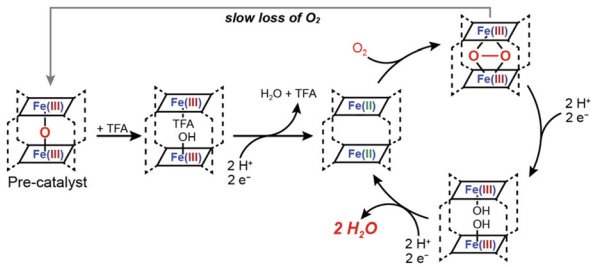

Scheme 2 Proposed mechanism of Oxygen Reduction Reaction catalyzed by Fe_2O prism.

is removed under acidic conditions, the dynamics of the two clipped prisms will differ. As with our Co_2 prisms, when shorter molecular clips are used, selectivities and kinetics are enhanced.[38] In addition, since both **Fe_2O Rhoxo**, and **Fe_2O Rh-benzo** preserve a cofacial arrangement in solution under acidic conditions despite the loss of the μ-oxo, our prisms are a rare example of dimeric ORR electrocatalysts that operate in homogenous conditions, which results in markedly different current responses. The selective and highly active **Fe_2O Rhoxo** operates in the "K region" of homogenous electrocatalysis wherein substrate is depleted.[51] The current response for **Fe_2O Rhoxo** does show evidence for some substrate depletion but more closely resembles the KS region prior to the onset of the plateau. The current response for **$(FeTPhP)_2O$** is actually due to monomeric FeTPhP that is generated by the acidic conditions and thus its curve is significantly different.

Conclusions

We have repurposed dinuclear molecular clips that have previously been used to drive coordination-driven self-assembly reactions to instead enable the post-assembly modification of cofacial porphyrins. Although bis-iron(III)-μ-oxo porphyrins already adopt a cofacial geometry, the use of molecular clips can have a significant impact on the reactivity of such species. Under acidic conditions, the μ-oxo bridge is rapidly severed and unclipped architectures quickly transform into two monomeric porphyrins. Our post-assembly modification preserves the cofacial arrangement under such conditions. A dinuclear cavity can be maintained *via* solid-state immobilization, yet even here the selectivity and activity of such species as electrocatalysts for ORR is still impacted by the introduction of molecular clips. We demonstrate that these effects are dependent on the length of the molecular clips. Our catalyst containing the shortest bridge, **Fe_2O Rhoxo**, cuts down the production of H_2O_2 by half relative to the longer **Fe_2O Rh-benzo** and unclipped **$(FeTPhP)_2O$** (7.2% *versus* ~15%). Thus, the design principles used for coordination self-assembly, where metal–ligand bond formation is the basis for the construction of complex polynuclear architectures, can readily be applied to tuning catalytic centers to enhance stability and reactivity.

Data availability

The data supporting this article have been included as part of the ESI.†

Author contributions

DZ spearheaded experimental work including synthesis, characterization, and reactivity studies and wrote the paper. LER conducted spectroelectrochemistry measurements. MRC carried out the calculations. TRC designed the research and wrote the paper. The manuscript was written through contributions of all authors. All authors have given approval to the final version of the manuscript.

Conflicts of interest

There are no conflicts to declare.

Acknowledgements

The authors thank Dr Alan Friedman for helpful discussions in collecting ESI-MS data. This work was supported by NSF CAREER Award #1847950 (TRC). Characterization work was performed in part in the Chemistry Instrument Center (CIC), University at Buffalo, SUNY, Buffalo, NY. This work used the 12T Bruker SolariXR 12 Hybrid FTMS with Imaging MALDI and Nano-LC supported by NSF S10RR029517.

References

1 S. Yoshikawa and A. Shimada, *Chem. Rev.*, 2015, **115**, 1936–1989.
2 S. W. Ragsdale, *Chem. Rev.*, 2006, **106**, 3317–3337.
3 J. B. Howard and D. C. Rees, *Chem. Rev.*, 1996, **96**, 2965–2982.
4 J. T. Groves, in *Cytochrome P450: Structure, Mechanism, and Biochemistry*, ed. P. R. Ortiz de Montellano, Springer US, Boston, MA, 2005, pp. 1–43. DOI: 10.1007/0-387-27447-2_1.
5 E. Y. Tshuva and S. J. Lippard, *Chem. Rev.*, 2004, **104**, 987–1012.
6 K.-Y. Wang, J. Zhang, Y.-C. Hsu, H. Lin, Z. Han, J. Pang, Z. Yang, R.-R. Liang, W. Shi and H.-C. Zhou, *Chem. Rev.*, 2023, **123**, 5347–5420.
7 I. Bhugun, D. Lexa and J.-M. Savéant, *J. Am. Chem. Soc.*, 1996, **118**, 3982–3983.
8 X. Li, H. Lei, L. Xie, N. Wang, W. Zhang and R. Cao, *Acc. Chem. Res.*, 2022, **55**, 878–892.
9 O. Kenichi, H. Agus, N. Junichiro, S. Hiroshi and T. Eishun, *Bull. Chem. Soc. Jpn.*, 2000, **73**, 1153–1163.
10 L. Xie, X.-P. Zhang, B. Zhao, P. Li, J. Qi, X. Guo, B. Wang, H. Lei, W. Zhang, U.-P. Apfel and R. Cao, *Angew. Chem., Int. Ed.*, 2021, **60**, 7576–7581.

11 S. Bhunia, A. Ghatak, A. Rana and A. Dey, *J. Am. Chem. Soc.*, 2023, **145**, 3812–3825.
12 A. Ghatak, S. Bhunia and A. Dey, *ACS Catal.*, 2020, **10**, 13136–13148.
13 S. Dey, B. Mondal, S. Chatterjee, A. Rana, S. Amanullah and A. Dey, *Nat. Rev. Chem.*, 2017, **1**, 0098.
14 B. Mondal, P. Sen, A. Rana, D. Saha, P. Das and A. Dey, *ACS Catal.*, 2019, **9**, 3895–3899.
15 D. J. Martin and J. M. Mayer, *J. Am. Chem. Soc.*, 2021, **143**, 11423–11434.
16 K. Guo, X. Li, H. Lei, H. Guo, X. Jin, X.-P. Zhang, W. Zhang, U.-P. Apfel and R. Cao, *Angew. Chem., Int. Ed.*, 2022, **61**, e202209602.
17 K. Guo, H. Lei, X. Li, Z. Zhang, Y. Wang, H. Guo, W. Zhang and R. Cao, *Chin. J. Catal.*, 2021, **42**, 1439–1444.
18 P. T. Smith, B. P. Benke, Z. Cao, Y. Kim, E. M. Nichols, K. Kim and C. J. Chang, *Angew. Chem., Int. Ed.*, 2018, **57**, 9684–9688.
19 J. S. Derrick, M. Loipersberger, S. K. Nistanaki, A. V. Rothweiler, M. Head-Gordon, E. M. Nichols and C. J. Chang, *J. Am. Chem. Soc.*, 2022, **144**, 11656–11663.
20 K. M. Kadish, G. Larson, D. Lexa and M. Momenteau, *J. Am. Chem. Soc.*, 1975, **97**, 282–288.
21 J. Rosenthal, B. J. Pistorio, L. L. Chng and D. G. Nocera, *J. Org. Chem.*, 2005, **70**, 1885–1888.
22 J. Rosenthal, T. D. Luckett, J. M. Hodgkiss and D. G. Nocera, *J. Am. Chem. Soc.*, 2006, **128**, 6546–6547.
23 E. A. Mohamed, Z. N. Zahran and Y. Naruta, *Chem. Commun.*, 2015, **51**, 16900–16903.
24 M. L. Pegis, D. J. Martin, C. F. Wise, A. C. Brezny, S. I. Johnson, L. E. Johnson, N. Kumar, S. Raugei and J. M. Mayer, *J. Am. Chem. Soc.*, 2019, **141**, 8315–8326.
25 J. P. Collman, C. M. Elliott, T. R. Halbert and B. S. Tovrog, *Proc. Natl. Acad. Sci. U. S. A.*, 1977, **74**, 18–22.
26 J. P. Collman, M. Marrocco, P. Denisevich, C. Koval and F. C. Anson, *J. Electroanal. Chem. Interfacial Electrochem.*, 1979, **101**, 117–122.
27 J. P. Collman, P. Denisevich, Y. Konai, M. Marrocco, C. Koval and F. C. Anson, *J. Am. Chem. Soc.*, 1980, **102**, 6027–6036.
28 Y.-J. Lin, Y.-F. Han and G.-X. Jin, *J. Organomet. Chem.*, 2012, **708–709**, 31–36.
29 W.-X. Gao, H.-N. Zhang and G.-X. Jin, *Coord. Chem. Rev.*, 2019, **386**, 69–84.
30 N. P. E. Barry, P. Govindaswamy, J. Furrer, G. Süss-Fink and B. Therrien, *Inorg. Chem. Commun.*, 2008, **11**, 1300–1303.
31 N. P. E. Barry, M. Austeri, J. Lacour and B. Therrien, *Organometallics*, 2009, **28**, 4894–4897.
32 S. P. Black, D. M. Wood, F. B. Schwarz, T. K. Ronson, J. J. Holstein, A. R. Stefankiewicz, C. A. Schalley, J. K. M. Sanders and J. R. Nitschke, *Chem. Sci.*, 2016, **7**, 2614–2620.
33 W. Meng, B. Breiner, K. Rissanen, J. D. Thoburn, J. K. Clegg and J. R. Nitschke, *Angew. Chem., Int. Ed.*, 2011, **50**, 3479–3483.
34 A. N. Oldacre, A. E. Friedman and T. R. Cook, *J. Am. Chem. Soc.*, 2017, **139**, 1424–1427.
35 A. N. Oldacre, M. R. Crawley, A. E. Friedman and T. R. Cook, *Chem. – Eur. J.*, 2018, **24**, 10984–10987.
36 M. R. Crawley, D. Zhang, A. N. Oldacre, C. M. Beavers, A. E. Friedman and T. R. Cook, *J. Am. Chem. Soc.*, 2021, **143**, 1098–1106.
37 M. R. Crawley, D. Zhang and T. R. Cook, *Inorg. Chem. Front.*, 2023, **10**, 316–324.
38 D. Zhang, M. R. Crawley, A. N. Oldacre, L. J. Kyle, S. N. MacMillan and T. R. Cook, *Inorg. Chem.*, 2023, **62**, 1766–1775.
39 D. Zhang, M. R. Crawley, M. Fang, L. J. Kyle and T. R. Cook, *Dalton Trans.*, 2022, **51**, 18373–18377.
40 C. J. Chang, E. A. Baker, B. J. Pistorio, Y. Deng, Z.-H. Loh, S. E. Miller, S. D. Carpenter and D. G. Nocera, *Inorg. Chem.*, 2002, **41**, 3102–3109.
41 B. J. Pistorio, C. J. Chang and D. G. Nocera, *J. Am. Chem. Soc.*, 2002, **124**, 7884–7885.
42 D.-H. Chin, G. N. La Mar and A. L. Balch, *J. Am. Chem. Soc.*, 1980, **102**, 4344–4350.
43 D.-H. Chin, G. N. La Mar and A. L. Balch, *J. Am. Chem. Soc.*, 1980, **102**, 5945–5947.
44 N. Mihara, Y. Yamada, H. Takaya, Y. Kitagawa, S. Aoyama, K. Igawa, K. Tomooka and K. Tanaka, *Chem. – Eur. J.*, 2017, **23**, 7508–7514.
45 O. Tamon, I. Masahiro, S. Takayoshi, K. Hisatoshi and K. Jitsuo, *Chem. Lett.*, 1986, **15**, 1467–1470.
46 O. Tamon, Y. Manabu, N. Takeo, K. Hisatoshi and K. Jitsuo, *Chem. Lett.*, 1982, **11**, 977–980.
47 S. Acosta-Calle and A. J. M. Miller, *Acc. Chem. Res.*, 2023, **56**, 971–981.
48 M.-N. Birkholz, Z. Freixa and P. W. N. M. van Leeuwen, *Chem. Soc. Rev.*, 2009, **38**, 1099–1118.
49 D. W. Thomas and A. E. Martell, *J. Am. Chem. Soc.*, 1959, **81**, 5111–5119.
50 E. B. Fleischer, *Inorg. Chem.*, 1962, **1**, 493–495.
51 E. S. Rountree, B. D. McCarthy, T. T. Eisenhart and J. L. Dempsey, *Inorg. Chem.*, 2014, **53**, 9983–10002.
52 N. Elgrishi, K. J. Rountree, B. D. McCarthy, E. S. Rountree, T. T. Eisenhart and J. L. Dempsey, *J. Chem. Educ.*, 2018, **95**, 197–206.
53 Y.-F. Han, Y.-J. Lin, L.-H. Weng, H. Berke and G.-X. Jin, *Chem. Commun.*, 2008, 350–352, DOI: **10.1039/B711809K**.
54 T. Schuh, O. Kataeva and H.-J. Knölker, *Chem. Sci.*, 2023, **14**, 257–265.
55 S. Grimme, A. Hansen, S. Ehlert and J.-M. Mewes, *J. Chem. Phys.*, 2021, **154**, 064103.
56 F. Neese, F. Wennmohs, U. Becker and C. Riplinger, *J. Chem. Phys.*, 2020, **152**, 224108.
57 P. A. Benavides, M. A. Gordillo, A. Yadav, M. A. Joaqui-Joaqui and S. Saha, *Chem. Sci.*, 2022, **13**, 4070–4081.
58 V. Vajpayee, S. Bivaud, S. Goeb, V. Croué, M. Allain, B. V. Popp, A. Garci, B. Therrien and M. Sallé, *Organometallics*, 2014, **33**, 1651–1658.